

Application of Tetrazole-Functionalized Thioethers with Different Spacer Lengths in the Self-Assembly of Polyoxometalate-Based Hybrid Compounds

Xiuli Wang,* Hailiang Hu, Aixiang Tian, Hongyan Lin, and Jin Li

Faculty of Chemistry and Chemical Engineering, Bohai University, Jinzhou 121000, People's Republic of China

Received April 28, 2010

Three metal–organic networks based on Keggin-type polyoxometalates (POMs) have been hydrothermally synthesized by tuning the spacer lengths of bis(tetrazole)-functionalized thioether ligands and structurally characterized: $[\text{Cu}_4(\text{bmtm})_4][\text{SiW}_{12}\text{O}_{40}] \cdot 2\text{H}_2\text{O}$ (**1**), $[\text{Cu}_4(\text{bmte})_{3.5}][\text{SiW}_{12}\text{O}_{40}]$ (**2**), and $[\text{Cu}_4(\text{btmp})_4][\text{SiW}_{12}\text{O}_{40}]$ (**3**) [bmtm = 1,1'-bis(1-methyl-5-mercapto-1,2,3,4-tetrazole)methane, bmte = 1,2-bis(1-methyl-5-mercapto-1,2,3,4-tetrazole)ethane, and btmp = 1,5-bis(1-methyl-5-mercapto-1,2,3,4-tetrazole)pentane]. The spacer lengths and sulfhydryl of bis(tetrazole)-functionalized thioether ligands play important roles in the final framework formation, as shown by X-ray diffraction analysis. In compound **1**, with the connection of a N,S bridge of bmtm, two kinds of binuclear Cu^{I} units are formed and linked to construct a one-dimensional (1D) chain. The $[\text{SiW}_{12}\text{O}_{40}]^{4-}$ (SiW_{12}) cluster provides four terminal O atoms linking four binuclear units to generate a two-dimensional layer with $(8^3)_2(8^5 \cdot 10)$ topology. In compound **2**, centrosymmetric octameric moieties composed of two equivalent tetrameric Cu^{I} units are bridged by bmte ligands to form a 1D chain. The SiW_{12} clusters show an unusual (2,8)-connected mode to connect with the 1D chain and construct a four-connected three-dimensional (3D) network with $5^3 \cdot 6^2 \cdot 7$ topology. Compound **3** exhibits a rare 3D host framework with a type of large cavity and two types of small windows. The SiW_{12} clusters as templates are strongly cemented into the large cavities and completely encircled by small windows. Furthermore, the compound **2** bulk-modified carbon-paste electrode (**2**-CPE) displays good electrocatalytic activity toward the reduction of nitrite.

Introduction

Recently, the design and synthesis of organic–inorganic hybrid multifunctional materials has been an area of rapid growth.¹ Polyoxometalates (POMs), as anionic early-transition-metal oxide clusters, have attracted extensive attention because of their intrinsic stability and catalytic, electrical, and optical properties.² In this aspect, a remarkable branch of coordination chemistry is the synthesis of POM-based hybrid materials. Up to now, several kinds of POMs have been introduced as templates and/or inorganic building units to

direct the formation of novel hybrid compounds, such as Keggin-type,³ Wells-Dawson-type,⁴ and octamolybdate clusters.⁵ Among many different types of POMs, the classical Keggin polyanions are the most widely recognized and

*To whom correspondence should be addressed. E-mail: wangxiuli@bhu.edu.cn. Tel.: +86-416-3400158.

(1) (a) Li, J. R.; Tao, Y.; Yu, Q.; Bu, X. H. *Chem. Commun.* **2007**, 1527. (b) Zou, J. P.; Peng, Q.; Wen, Z. H.; Zeng, G. S.; Xing, Q. J.; Guo, G. C. *Cryst. Growth Des.* **2010**, *10*, 2613. (c) Liao, T. B.; Ling, Y.; Chen, Z. X.; Zhou, Y. M.; Weng, L. H. *Chem. Commun.* **2010**, *46*, 1100. (d) Kennedy, S.; Karotsis, G.; Beavers, C. M.; Teat, S. J.; Brechin, E. K.; Dalgarno, S. J. *Angew. Chem., Int. Ed.* **2010**, *49*, 1. (e) Huang, F. P.; Tian, J. L.; Li, D. D.; Chen, G. J.; Gu, W.; Yan, S. P.; Liu, X.; Liao, D. Z.; Cheng, P. *Inorg. Chem.* **2010**, *49*, 2525. (f) Liang, X. Q.; Li, D. P.; Li, C. H.; Zhou, X. H.; Li, Y. Z.; Zuo, J. L.; You, X. Z. *Cryst. Growth Des.* **2010**, *10*, 2596.

(2) (a) Khenkin, A. M.; Neumann, R. *J. Am. Chem. Soc.* **2002**, *124*, 4198. (b) Volkmer, D.; Bredenköter, B.; Tellenbröcker, J.; Kögerler, P.; Kurth, D. G.; Lehmann, P.; Schnablegger, H.; Schwahn, D.; Piepenbrink, M.; Krebs, B. *J. Am. Chem. Soc.* **2002**, *124*, 10489. (c) Zhang, Y. J.; Shen, Y. F.; Yuan, J. H.; Han, D. X.; Wang, Z. J.; Zhang, Q. X.; Niu, L. *Angew. Chem., Int. Ed.* **2006**, *45*, 5867. (d) Kögerler, P.; Cronin, L. *Angew. Chem., Int. Ed.* **2005**, *44*, 844. (e) Mishra, P. P.; Pigga, J.; Liu, T. B. *J. Am. Chem. Soc.* **2008**, *130*, 1548.

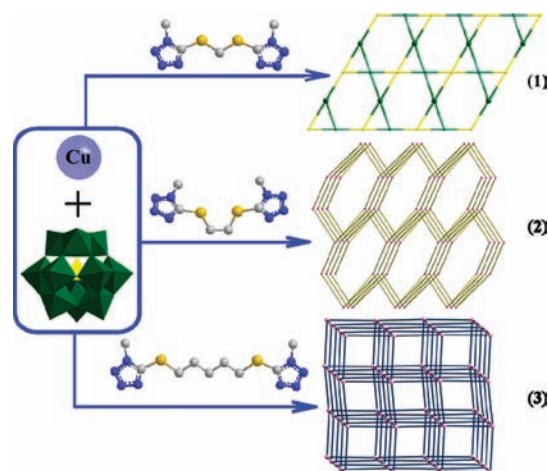
(3) (a) Reinoso, S.; Vitoria, P.; Gutiérrez-Zorrilla, J. M.; Lezama, L.; Felices, L. S.; Beitia, J. I. *Inorg. Chem.* **2005**, *44*, 9731. (b) Reinoso, S.; Vitoria, P.; Gutiérrez-Zorrilla, J. M.; Lezama, L.; Madariaga, J. M.; Felices, L. S.; Iturraspe, A. *Inorg. Chem.* **2007**, *46*, 4010. (c) Ren, Y. P.; Kong, X. J.; Long, L. S.; Huang, R. B.; Zheng, L. S. *Cryst. Growth Des.* **2006**, *6*, 572. (d) Ren, Y. P.; Kong, X. J.; Hu, X. Y.; Sun, M.; Long, L. S.; Huang, R. B.; Zheng, L. S. *Cryst. Growth Des.* **2006**, *45*, 4016. (e) Kong, X. J.; Ren, Y. P.; Zheng, P. Q.; Long, Y. X.; Long, L. S.; Huang, R. B.; Zheng, L. S. *Inorg. Chem.* **2006**, *45*, 10702. (f) Zhang, C. J.; Chen, Y. G.; Pang, H. J.; Shi, D. M.; Hu, M. X.; Li, J. *Inorg. Chem. Commun.* **2008**, *11*, 765. (g) Yuan, L.; Qin, C.; Wang, X. L.; Wang, E. B.; Chang, S. *Eur. J. Inorg. Chem.* **2008**, 4936. (h) Dai, L. M.; You, W. S.; Wang, E. B.; Wu, S. X.; Su, Z. M.; Du, Q. H.; Zhao, Y.; Fang, Y. *Cryst. Growth Des.* **2009**, *9*, 2110. (4) (a) Tian, A. X.; Han, Z. G.; Sha, J. Q.; Zhai, J. L.; Zhang, P. P.; Chen, J.; Liu, H. S. *Z. Anorg. Allg. Chem.* **2007**, *633*, 2730. (b) Sha, J. Q.; Wang, C.; Peng, J.; Chen, J.; Tian, A. X.; Zhang, P. P. *Inorg. Chem. Commun.* **2007**, *10*, 1321. (c) Zhang, C. D.; Liu, S. X.; Sun, C. Y.; Ma, F. J.; Su, Z. M. *Cryst. Growth Des.* **2009**, *9*, 3655. (d) Yang, H. X.; Guo, S. P.; Tao, J.; Lin, J. X.; Cao, R. *Cryst. Growth Des.* **2009**, *9*, 4735. (e) Wang, X. L.; Hu, H. L.; Tian, A. X.; Lin, H. Y.; Li, J.; Shi, L. M. *Inorg. Chem. Commun.* **2010**, *13*, 745.

(5) (a) Hagrman, D.; Zapf, P. J.; Zubieta, J. *Chem. Commun.* **1998**, 1283. (b) Hagrman, D.; Zubieta, J. *Chem. Commun.* **1998**, 2005. (c) Lan, Y. Q.; Li, S. L.; Wang, X. L.; Shao, K. Z.; Du, D. Y.; Zang, H. Y.; Su, Z. M. *Inorg. Chem.* **2008**, *47*, 8179. (d) Han, Z. G.; Gao, Y. Z.; Hu, C. W. *Cryst. Growth Des.* **2008**, *8*, 1261. (e) Zhang, X. T.; Wei, P. H.; Sun, D. F.; Ni, Z. H.; Dou, J. M.; Li, B.; Shi, C. W.; Hu, B. *Cryst. Growth Des.* **2009**, *9*, 4424.

thoroughly studied, and they have been regarded as important building units in the self-assembly of hybrid materials. Our group has reported several novel hybrid compounds based on Keggin polyanions and Cu ions.⁶ As an ongoing effort, we want to develop the strategy of Keggin-type POM-based hybrid compounds by exploring proper organic subunits. Among the large amount of reported works, the introduction of flexible organic ligands to the POM-based system is of particular interest.⁷ The main reason lies in the flexibility and conformational freedom of such organic components that allow them to conform to the coordination environments of metal ions and POMs.⁸ Many POM-based novel structures constructed from flexible organic ligands have been obtained to date.⁹ However, upon a search of the CSD database, it is found that the reported flexible ligands used in these systems are almost always those with $-(CH_2)_n-$ as their backbones. When these kinds of ligands coordinate with metal centers, to some extent their backbones can bend to satisfy the coordination request because of their flexibility. However, the twist degree of such ligands is restricted by the nature of the $-(CH_2)_n-$ group. The constraint of these ligands inspires us to explore more ductile organic ligands to construct novel structures. Thus, a kind of remarkable “soft” thioether based on tetrazole attracts our attention. Compared with the ligands containing $-(CH_2)_n-$ groups, the ligands containing sulfhydryl exhibit better flexibility and can bend to a larger twist degree.¹⁰ Theoretically, this character would be observed when the backbones $-(CH_2)_n-$ are decorated by S atoms, so that intriguing structures should be expected.

Given the above aspects, we introduce sulfhydryl into flexible organic ligands, and three structurally related bis-(tetrazole)-functionalized thioethers [1,1'-bis(1-methyl-5-mercapto-1,2,3,4-tetrazole)methane (bmtm), 1,2-bis(1-methyl-5-mercapto-1,2,3,4-tetrazole)ethane (bmte), and 1,5-bis(1-methyl-5-mercapto-1,2,3,4-tetrazole)pentane (bmtpp)] are designed. Compared with commonly used organic subunits, these kinds of ligands have more advantages: (i) They have more flexible backbones owing to the introduction of sulfhydryl. (ii) They

Scheme 1



possess more potential coordination sites provided by tetrazole groups and S atoms. These features make them attractive for the design of novel POM-based hybrids with interesting structures. To the best of our knowledge, research on the introduction of tetrazole-functionalized thioethers into POM systems has not been reported up to now.

In this paper, the heterocyclic thioether derivatives bmtm, bmte, and bmtpp have been employed to construct Keggin-type POM-based hybrid compounds. Three $[SiW_{12}O_{40}]^{4-}$ -based compounds with unique structures, namely, $[Cu_4(bmtm)_4][SiW_{12}O_{40}] \cdot 2H_2O$ (1), $[Cu_4(bmte)_{3.5}][SiW_{12}O_{40}]$ (2), and $[Cu_4(bmtpp)_4][SiW_{12}O_{40}]$ (3), have been obtained under hydrothermal conditions (Scheme 1). The influence of the ligand spacer length on the structure is discussed, and the electrochemical behavior of compound 2 is reported.

Experimental Section

Materials and Methods. All chemicals were reagent grade and were used as received from commercial sources without further purification. The ligands bmtm, bmte, and bmtpp were prepared according to the literature method.¹¹ Elemental analyses (C, H, and N) were carried out on a Perkin-Elmer 240C elemental analyzer. Fourier transform IR spectra (KBr pellets) were taken on a Magna FT-IR 560 spectrometer. X-ray photoelectron spectroscopy (XPS) analyses were performed on a VG ESCA-LAB MK II spectrometer with a Mg K α radiation (1253.6 eV) achromatic X-ray source. The vacuum inside the analysis chamber was maintained at 6.2×10^{-6} Pa during analysis. Thermogravimetric analysis (TGA) was carried out with a Pyris Diamond TGA/DTA instrument in flowing N_2 with a heating rate of 10 °C/min. A CHI 440 electrochemical workstation connected to a Digital-586 personal computer was used for control of the electrochemical measurements and for data collection. A conventional three-electrode system was used. A saturated calomel electrode (SCE) was used as the reference electrode and a platinum wire as the counter electrode. The title compound chemically bulk-modified carbon-paste electrodes (CPEs) were used as the working electrode.

Synthesis of $[Cu_4(bmtm)_4][SiW_{12}O_{40}] \cdot 2H_2O$ (1). A mixture of $H_4SiW_{12}O_{40} \cdot 26H_2O$ (0.20 g, 0.07 mmol), $Cu(OAc)_2 \cdot H_2O$ (0.12 g, 0.60 mmol), and bmtm (0.049 g, 0.20 mmol) was dissolved in 10.0 mL of distilled water. When the pH value was adjusted to about 3.5 with 1 M HCl, the mixture was sealed into a 20-mL Teflon-lined autoclave and heated to 160 °C in 100 min.

(11) She, J. B.; Zhang, G. F.; Dou, Y. L.; Fan, X. Z.; Li, J. Z. *Acta Crystallogr.* **2006**, E62, o402.

(6) (a) Wang, X. L.; Bi, Y. F.; Chen, B. K.; Lin, H. Y.; Liu, G. C. *Inorg. Chem.* **2008**, 47, 2442. (b) Wang, X. L.; Lin, H. Y.; Bi, Y. F.; Chen, B. K.; Liu, G. C. *J. Solid State Chem.* **2008**, 181, 556.

(7) (a) La Duca, R. L., Jr.; Ratkoski, R.; Rarig, R. S., Jr.; Zubieta, J. *Inorg. Chem. Commun.* **2008**, 4, 621. (b) Tian, A. X.; Ying, J.; Peng, J.; Sha, J. Q.; Pang, H. J.; Zhang, P. P.; Chen, Y.; Zhu, M.; Su, Z. M. *Cryst. Growth Des.* **2008**, 8, 3717. (c) Tian, A. X.; Ying, J.; Peng, J.; Sha, J. Q.; Han, Z. G.; Ma, J. F.; Su, Z. M.; Hu, N. H.; Jia, H. Q. *Inorg. Chem.* **2008**, 47, 3274. (d) Li, S. L.; Lan, Y. Q.; Ma, J. F.; Yang, J.; Wang, X. H.; Su, Z. M. *Inorg. Chem.* **2007**, 46, 8283. (e) Dong, B. X.; Xu, Q. *Inorg. Chem.* **2009**, 48, 5861.

(8) (a) Tian, A. X.; Ying, J.; Peng, J.; Sha, J. Q.; Zhu, D. X.; Pang, H. J.; Zhang, P. P.; Chen, Y.; Zhu, M. *Inorg. Chem. Commun.* **2008**, 11, 1132. (b) Dong, B. X.; Peng, J.; Gómez-García, C. J.; Benmansour, S.; Jia, H. Q.; Hu, N. H. *Inorg. Chem.* **2007**, 46, 5933.

(9) (a) Sha, J. Q.; Peng, J.; Liu, H. S.; Chen, J.; Tian, A. X.; Zhang, P. P. *Inorg. Chem.* **2007**, 46, 11183. (b) Qi, Y. F.; Xiao, D. R.; Wang, E. B.; Zhang, Z. M.; Wang, X. L. *Aust. J. Chem.* **2007**, 60, 871. (c) Lan, Y. Q.; Li, S. L.; Su, Z. M.; Shao, K. Z.; Ma, J. F.; Wang, X. L.; Wang, E. B. *Chem. Commun.* **2008**, 58. (d) Lan, Y. Q.; Li, S. L.; Wang, X. L.; Shao, K. Z.; Du, D. Y.; Su, Z. M.; Wang, E. B. *Chem.—Eur. J.* **2008**, 14, 9999. (e) Qin, C.; Wang, X. L.; Wang, E. B.; Su, Z. M. *Inorg. Chem.* **2008**, 47, 5555. (f) Qin, C.; Wang, X. L.; Yuan, L.; Wang, E. B. *Cryst. Growth Des.* **2008**, 8, 2093. (g) Li, S. L.; Lan, Y. Q.; Ma, J. F.; Yang, J.; Liu, J.; Fu, Y. M.; Su, Z. M. *Dalton Trans.* **2008**, 2015. (h) Dong, B. X.; Xu, Q. *Cryst. Growth Des.* **2009**, 9, 2776. (i) Wang, X. L.; Qin, C.; Wang, E. B.; Su, Z. M. *Chem. Commun.* **2007**, 4245.

(10) (a) Zheng, Y.; Du, M.; Li, J. R.; Zhang, R. H.; Bu, X. H. *Dalton Trans.* **2003**, 1509. (b) Hanton, L. R.; Lee, K. J. *Chem. Soc., Dalton Trans.* **2000**, 1161. (c) Carballo, R.; Covelo, B.; Fernández-Hermida, N.; García-Martínez, E.; Lago, A. B.; Vázquez-López, E. M. *Cryst. Growth Des.* **2008**, 8, 995.

The autoclave was kept at 160 °C for 3 days and then slowly cooled to room temperature at a rate of 10 °C/h. Orange needle crystals of **1** were filtered and washed with distilled water (yield of about 32% based on W). Elem anal. Calcd for $C_{20}H_{36}Cu_4N_{32}O_{42}S_8SiW_{12}$: C, 5.80; H, 0.87; N, 10.82. Found: C, 5.73; H, 0.85; N, 10.95. IR (KBr pellet, cm^{-1}): 3672(s), 2360(s), 1672(w), 1508(m), 1400(s), 1222(m), 1180(s), 1012(m), 968(s), 920(s), 883(m), 800(s).

Synthesis of $[Cu_4(bmte)_{3.5}(SiW_{12}O_{40})]$ (2**).** Compound **2** was prepared in a manner similar to that for **1**, but the ligand bmte (0.052 g, 0.20 mmol) was used instead of bmtm. The pH was adjusted to about 4.2 with 1 M HCl. After the mixture was cooled to room temperature, orange block crystals of **2** were filtered and washed with distilled water (yield of about 40% based on W). Elem anal. Calcd for $C_{21}H_{35}Cu_4N_{28}O_{40}S_7SiW_{12}$: C, 6.25; H, 0.87; N, 9.72. Found: C, 6.21; H, 0.92; N, 9.80. IR (KBr pellet, cm^{-1}): 3435(s), 1627(s), 1471(m), 1404(s), 1180(s), 1012(m), 972(s), 921(s), 883(m), 800(s).

Synthesis of $[Cu_4(bmtm)_4(SiW_{12}O_{40})]$ (3**).** Compound **3** was prepared in a manner similar to that for **1**, but the ligand bmtm (0.060 g, 0.20 mmol) was used instead of bmtm. The pH was adjusted to about 4.2 with 1 M HCl. After the mixture was cooled to room temperature, pale-green crystals of **3** were filtered and washed with distilled water (yield of about 38% based on W). Elem anal. Calcd for $C_{36}H_{64}Cu_4N_{32}O_{40}S_8SiW_{12}$: C, 9.98; H, 1.48; N, 10.35. Found: C, 9.86; H, 1.36; N, 10.43. IR (KBr pellet, cm^{-1}): 2360(s), 1635(w), 1404(s), 1276(m), 1188(s), 1010(m), 968(s), 921(s), 883(m), 798(s).

Preparation of 1-, 2-, and 3-CPE. The compound **1** modified carbon paste electrode (1-CPE) was fabricated as follows: 0.03 g of compound **1** and 0.5 g of graphite powder were mixed and ground together by an agate mortar and pestle for approximately 20 min to achieve an even, dry mixture; to the mixture was added 0.20 mL of paraffin oil, and the resulting mixture was stirred with a glass rod; then the homogenized mixture was used to pack a 3 mm-inner-diameter glass tube to a length of 0.8 cm. Electrical contact was established with the copper stick, and the surface of 1-CPE was wiped with weighing paper. In a similar manner, 2- and 3-CPE were made with compounds **2** and **3**.

X-ray Crystallographic Measurements. Single-crystal X-ray diffraction (XRD) data for compounds **1–3** were collected on a Bruker Smart 1000 CCD diffractometer with Mo K α radiation ($\lambda = 0.71073 \text{ \AA}$) by ω and θ scan modes at 296 K. The structures were solved by direct methods and refined on F^2 by full-matrix least squares using the *SHELXL* package.¹² All of the non-H atoms were refined anisotropically. The positions of the H atoms on the C or N atoms were calculated theoretically. Relatively, the high R1 and wR2 factors of compound **1** might be due to the weak high-angle diffractions and the disorder of the POM atoms. These features seem to be intrinsic to compound **1**, as indicated by several measurements on crystals from different batches. A summary of the crystallographic data and structural refinements for compounds **1–3** is given in Table 1. Selected bond distances (Å) and angles (deg) of the three compounds are listed in Table S1 (Supporting Information). Crystallographic data for the structures have been deposited at the Cambridge Crystallographic Data Centre as CCDC 763404 for **1**, 763405 for **2**, and 763406 for **3**. The coordinates can be obtained, upon request, from the Director, Cambridge Crystallographic Data Centre, 12 Union Road, Cambridge CB2 1EZ, U.K.

Results and Discussion

Synthesis. Compounds **1–3** were synthesized under similar hydrothermal conditions, except for using sulfhydryl-containing bis(tetrazole) ligands with different spacer lengths. Parallel experiments show that the initial reactants

Table 1. Crystal Data and Structural Refinements for Compounds **1–3**

	1	2	3
empirical formula	$C_{20}H_{36}Cu_4N_{32}O_{42}S_8SiW_{12}$	$C_{21}H_{35}Cu_4N_{28}O_{40}S_7SiW_{12}$	$C_{36}H_{64}Cu_4N_{32}O_{40}S_8SiW_{12}$
fw	4141.74	4032.64	4330.12
cryst syst	triclinic	triclinic	monoclinic
space group	$P\bar{1}$	$P\bar{1}$	$P2_1/c$
<i>a</i> (Å)	12.3635(13)	13.784(2)	13.294(2)
<i>b</i> (Å)	13.2905(14)	15.939(3)	25.171(4)
<i>c</i> (Å)	13.9050(15)	17.512(3)	13.626(2)
α (deg)	88.053(2)	79.346(2)	90
β (deg)	68.583(1)	81.562(2)	104.600(2)
γ (deg)	64.326(1)	79.064(2)	90
<i>V</i> (Å ³)	1895.9(3)	3687.5(11)	4412.3(12)
<i>Z</i>	1	2	2
<i>D_c</i> (g/m ³)	3.628	3.632	3.259
μ (mm ⁻¹)	19.554	20.071	16.811
<i>F</i> (000)	1862.0	3614.0	3940.0
collected reflns	9602	18 673	22 112
unique reflns	6587	12 814	7844
obsd reflns	5938	7680	5328
no. of param	584	1057	623
<i>R</i> _{int}	0.056	0.110	0.101
GOF	1.371	0.969	1.000
<i>R</i> ¹ [<i>I</i> > 2 σ (<i>I</i>)]	0.118	0.058	0.047
w <i>R</i> ² (all data)	0.279	0.130	0.111

$$^a R1 = \sum ||F_o| - |F_c|| / \sum |F_o|. \quad ^b wR2 = \sum [w(F_o^2 - F_c^2)^2] / \sum [w(F_o^2)^2]^{1/2}.$$

and the pH values of the reaction system are crucial for formation of the title compounds. Compounds **1–3** could only be obtained in the special pH values of 3.5 for **1** and 4.2 for **2** and **3**. When it was lower or higher than those special values, we could not obtain the expected single crystal. Meanwhile, if the reactant Cu(OAc)₂ was replaced by CuCl₂ or Cu(NO₃)₂, no crystalline phase was obtained but only precipitate, which indicated that acetate plays an important role in the formation of the title compounds. Bond valence sum calculations¹³ show that all W atoms are in the VI+ oxidation state and all Cu atoms are in the I+ oxidation state. The XPS spectra of compounds **1–3** (Figure S1 in the Supporting Information) further confirm the results of bond valence sum calculations. The presence of Cu^I in all three compounds indicates that the reactant Cu^{II} ions are probably reduced by organic ligands. Such a phenomenon is often observed in N-donor ligand/Cu^{II}/POM reaction systems under hydrothermal conditions.^{7c,9i,14} The four central μ_4 -O atoms of the $[SiW_{12}O_{40}]^{4-}$ anions (abbreviated to SiW₁₂) are disordered over eight positions in compounds **1–3**, which is not unusual in POM structures.

Crystal Structure of Compound 1. Crystal structure analysis reveals that compound **1** consists of half of a Keggin-type SiW₁₂ anion, two Cu^I ions, two types of bmtm ligands (bmtm¹ and bmtm²), and one lattice water molecule (Figure 1).

In compound **1**, there are two crystallographically independent Cu ions (Cu1 and Cu2), which exhibit two kinds of coordination geometries. The Cu1 ion adopts a four-coordinated trigonal-pyramidal geometry of $[Cu(1)N_3O]$ by three N atoms of two bmtm¹ ligands and one O atom of the SiW₁₂ cluster. The Cu2 ion is five-coordinated by three N atoms of two bmtm² ligands, one O atom of the SiW₁₂ cluster, and

(13) Brown, I. D.; Altermatt, D. *Acta Crystallogr., Sect. B* **1985**, *41*, 244.

(14) (a) Hagrman, D.; Zubieta, C.; Rose, D. J.; Zubieta, J.; Haushalter, R. C. *Angew. Chem., Int. Ed.* **1997**, *36*, 873. (b) Qu, X. S.; Xu, L.; Gao, G. G.; Li, F. Y.; Yang, Y. Y. *Inorg. Chem.* **2007**, *46*, 4775. (c) Liu, C. M.; Zhang, D. Q.; Zhu, D. B. *Cryst. Growth Des.* **2006**, *6*, 524. (d) Sha, J. Q.; Peng, J.; Liu, H. S.; Chen, J.; Dong, B. X.; Tian, A. X.; Su, Z. M. *Eur. J. Inorg. Chem.* **2007**, 1268.

(12) (a) Sheldrick, G. M. *SHELXS-97, Program for the Solution of Crystal Structure*; University of Göttingen: Göttingen, Germany, 1997. (b) Sheldrick, G. M. *SHELXL-97, Program for the Refinement of Crystal Structure*; University of Göttingen: Göttingen, Germany, 1997.

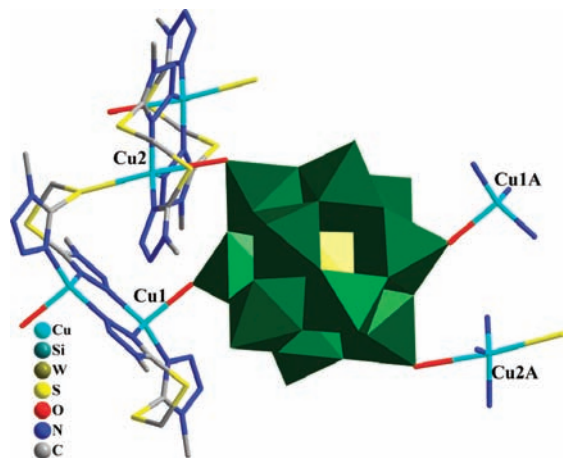


Figure 1. Stick/polyhedral view of the asymmetric unit of **1**. All H atoms and free lattice water molecule are omitted for clarity.

one S atom of the bmtm¹ ligand in a trigonal-bipyramidal geometry of [Cu₂N₃OS]. The bond distances around Cu1 are normal. Two weak coordination interactions [Cu2–O6 2.750(3) Å and Cu2–S2 2.835(16) Å] are observed within the [Cu₂N₃OS] moiety. Although the corresponding distances are very long, we consider that these bonds exist¹⁵ and play an important role in extending the dimensionality of compound **1**. It is worth to mentioning here that the Cu–S bond observed in POM chemistry is scarce.

Dramatic changes induced by a soft S atom and a tetrazole ring have been observed. (i) The introduction of S atoms leads to a more flexible backbone of the ligand, so the bmtm ligand can twist more easily to chelate a Cu^I ion. (ii) The bmtm ligand with eight potential coordination sites (six N donors and two S donors) exhibits versatile coordination modes (Table 2). The combination of the two features results in the formation of two types of binuclear secondary building units (SBUs; Figure S2 in the Supporting Information). The first one (SBU-1) is formed by a pair of symmetry-related Cu^I ions. One bmtm¹ ligand connects two Cu^I ions with three N atoms from its two terminal tetrazole rings: two N atoms (N1 and N5) from different tetrazole rings chelate one Cu^I ion, forming an eight-membered ring; another two N atoms (N1 and N2) from one tetrazole ring bridge two Cu^I ions, and two symmetrical bridges form a stable six-membered centrosymmetric binuclear ring. The second one (SBU-2) is formed by a pair of symmetry-related Cu^I ions.

The bmtm² ligand act as a tridentate $\mu_2(\eta^1, \eta^2)$ linkage, adopting a coordination mode similar to what bmtm¹ does within SBU-1. However, besides using three N atoms to connect two Cu^I ions, the bmtm¹ ligand employs a S atom to bridge the third Cu^I ion, i.e., a neighboring Cu2 ion from SBU-2. We define this coordination mode as a tetradentate $\mu_3(\eta^1, \eta^2, \eta^1_s)$ one. With the connection of such a S bridge, the two kinds of binuclear units, SBU-1 and SBU-2, are linked in a point-to-face fashion and alternately arrayed to form a wavelike chain (Figure 2).

The SiW₁₂ cluster provides four terminal O atoms linking four SBUs to generate a two-dimensional (2D) layer with (8³)₂(8⁵·10) topology, as shown in Figure 3a. Furthermore, the layers are parallel to each other and arranged in a stagger-peaked fashion. Through hydrogen-bonding interactions between SBUs and SiW₁₂ anions, a stairlike three-dimensional (3D) supramolecular framework is formed (Figure 3b).

Crystal Structure of Compound 2. Crystal structure analysis reveals that compound **2** exhibits a 3D framework, which is constructed by the halves of SiW₁₂ anions, four crystallographically independent Cu^I ions, and four bmtm ligands in the asymmetric unit (Figure 4). Similar to the Cu^I ions in **1**, the four Cu^I ions exhibit two kinds of coordination geometries, that is, trigonal-pyramidal geometry of [CuN₃O] for the Cu1, Cu3, and Cu4 ions and trigonal-bipyramidal geometry of [CuN₃O₂] for the Cu2 ion. The bond distances around the Cu^I ions are normal.

In compound **2**, the bmtm ligand exhibits diverse coordination modes (Table 2): (i) a tetradentate $\mu_3(\eta^1, \eta^3)$ linkage of bmtm¹, binding three Cu^I ions with four N atoms in an unusual asymmetrical mode; (ii) a tetradentate $\mu_3(\eta^2, \eta^2)$ linkage of bmtm², bridging two Cu^I ions and chelating one Cu^I ion with two apical N atoms, respectively; (iii) a tridentate $\mu_3(\eta^1, \eta^2)$ linkage of bmtm³, bridging three Cu^I ions with three apical N atoms in an asymmetrical mode; (iv) a bidentate $\mu_2(\eta^1, \eta^1)$ linkage of bmtm⁴, bridging two Cu^I ions (Cu4 and Cu4A) with two symmetrical N atoms (N26 and N26A). The observation of multicoordination modes coexisting in one structure is scarce.¹⁶

A tetrameric SBU (SBU-3; Figure S3 in the Supporting Information) is observed that is the second feature of compound **2**. Four types of bmtm molecules link four Cu^I ions (Cu1, Cu2, Cu3, and Cu4) to form a tetrameric unit, which contains two distinct nine-membered rings, two stable six-membered rings with one shared edge, and a stable five-membered ring. Linked by bridging bmtm ligands between the Cu4 atoms, two equivalent tetrameric SBU-3 form a centrosymmetric octameric moiety. Such octameric moieties are further bridged together by a bmtm ligand into a one-dimensional (1D) trainlike arrangement (Figure 5).


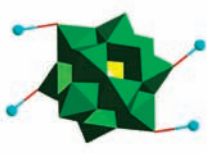
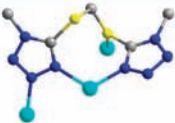

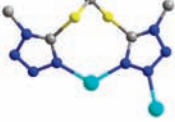

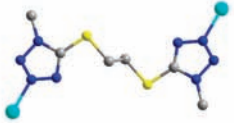


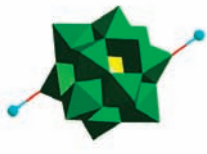
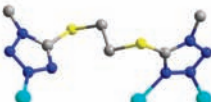

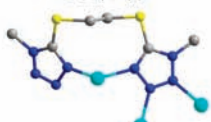

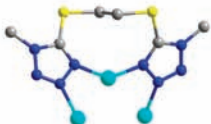


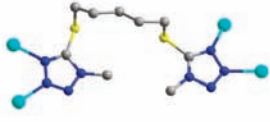

The third structural feature lies on SiW₁₂ anions, which exhibit versatile coordination modes. The Si₍₁₎W₁₂ clusters act as bidentate inorganic ligands bridging two Cu2 ions with two terminal O atoms, while the Si₍₂₎W₁₂ clusters act as tetradentate ligands coordinating to eight Cu^I ions with four terminal O atoms in a bridging style; this is the first observation of the tetradentate $\mu_8(\eta^2, \eta^2, \eta^2, \eta^2)$, eight-connected mode of SiW₁₂ anions. Integration of the two connection modes of SiW₁₂ anions brings a (2,8)-connected fashion, which has never been observed before. To our knowledge, compound **2** represents the highest connection number of saturated Keggin-type POMs to date.

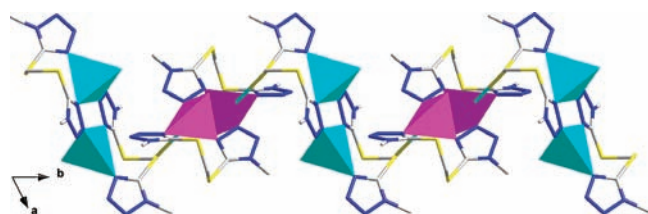
Finally, the combination of these three structural features induces a complicated 3D network. If the tetrameric SBU-3 are assigned as nodes and the SiW₁₂ clusters and

(15) (a) Prochaska, H. J.; Schwindinger, W. F.; Schwartz, M.; Burk, M. J.; Bernarducci, E.; Lalancette, R. A.; Potenza, J. A.; Schugar, H. J. *J. Am. Chem. Soc.* **1982**, *103*, 3446. (b) Yang, H. X.; Li, G. L.; Xu, B.; Liu, T. F.; Li, Y. F.; Cao, R.; Batten, S. R. *Inorg. Chem. Commun.* **2009**, *12*, 605. (c) Lisnard, L.; Dolbecq, A.; Mialane, P.; Marrot, J.; Codjovi, E.; Sécherresse, F. *Dalton Trans.* **2005**, 3913.

(16) Tian, A. X.; Ying, J.; Peng, J.; Sha, J. Q.; Pang, H. J.; Zhang, P. P.; Chen, Y.; Zhu, M.; Su, Z. M. *Inorg. Chem.* **2009**, *48*, 100.

Table 2. Coordination Sites of SiW_{12} , Coordination Number and Modes of L (L = bmtm, bmte, and bmtp), and Cu Ions in Compounds 1–3

crystal photo	coordination sites of POM	coordination number and modes of L	coordination number and modes of copper ions
Compound 1 		 $\mu_3(\eta^1, \eta^2, \eta^1_s)$	
		 $\mu_2(\eta^1, \eta^2)$	
		 $\mu_2(\eta^1, \eta^1)$	
Compound 2 		 $\mu_3(\eta^1, \eta^2)$	
		 $\mu_3(\eta^1, \eta^3)$	
		 $\mu_3(\eta^2, \eta^2)$	
Compound 3 		 $\mu_4(\eta^2, \eta^2)$	

**Figure 2.** Wavelike chain of compound 1.

the bridging $\text{bmtm}^3/\text{bmte}^4$ molecules as connectors, the overall framework becomes a four-connected network with $5^3 \cdot 6^2 \cdot 7$ topology (Figure 6).

Crystal Structure of Compound 3. Crystal structure analysis reveals that compound 3 is also a 3D framework. As shown in Figure 7, the asymmetric unit is built up from one SiW_{12} anion, two Cu^{I} ions, and two bmtm ligands.

The two Cu^{I} ions are similarly four-coordinated by four N atoms from the bmtm ligands to form two cationic structural cores, $[\text{Cu}_{(1)}(\mu_4\text{-bmtm})_4]^+$ and $[\text{Cu}_{(2)}(\mu_4\text{-bmtm})_4]^+$, in which the bmtm ligands act as tetradentate $\mu_4(\eta^2, \eta^2)$ linkages to coordinate to Cu^{I} in a seesaw fashion. Bridged by tetrazole rings of bmtm, the two distinct cationic cores are perpendicularly linked and alternately arrayed to form a 1D chain (Figure 8a). Moreover, the Cu axis of each 1D chain

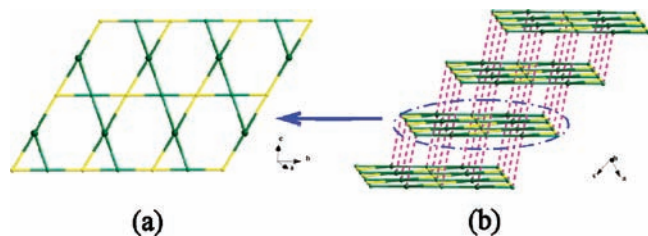


Figure 3. Trinodal ($3^2 \cdot 6^2 \cdot 8^2$) net (a) and the stairlike 3D supramolecular framework (b) of compound **1** viewed along a given direction.

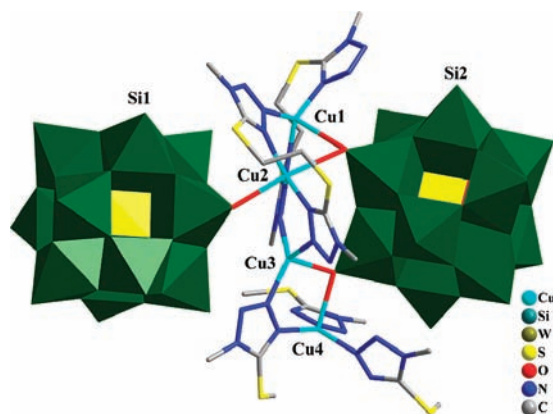


Figure 4. Stick/polyhedral view of the asymmetric unit of **2**. H atoms are omitted for clarity.

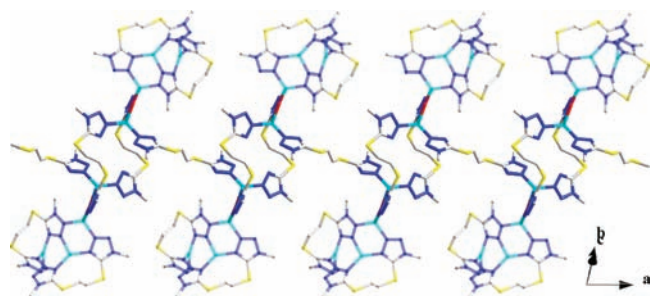


Figure 5. Trainlike chain in compound **2**.

lies on an inversion center (Figure 8b) and interlocks with four neighbors through flexible backbones of bmtp ligands. The overall result of such a structural organization leads to an infinite 3D host metal–organic framework with a large cavity (A type, the corresponding edge distances between the copper vertices are 12.9×13.4 Å). Interestingly, two types of narrow windows are simultaneously present within the framework: a trapezoidal slot (4.2×4.8 Å, B type) and a parallelogram mesh (4.0×5.0 Å, C type). The tetrazole methyl groups are accommodated in them. These small windows could be well recognized as a self-complementary of crystal stability. Moreover, the two types of small windows run along the Cu axis, leading to its radial arrangement around each Cu axis. The SiW_{12} clusters as templates are strongly cemented into the A-type cavities and completely encircled by B- and C-type windows, as shown in Figure 9 (left). If the $[\text{Cu}_3(\mu_4\text{-bmtp})_8]^{3+}$ subunits are taken as nodes (Figure S4 in the Supporting Information), a six-connected architecture with a primitive (α -Po) net is generated, in which the subunit nodes are connected via the

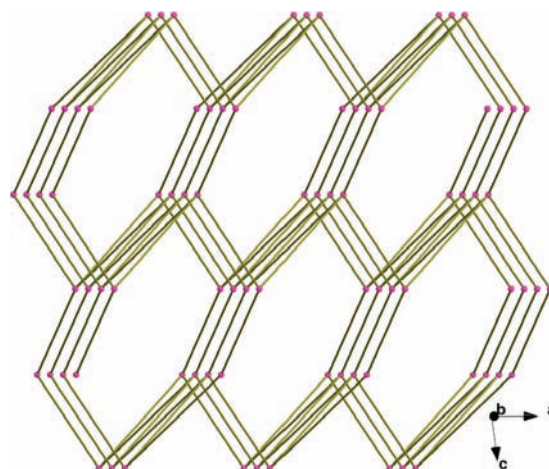


Figure 6. View of the topology of compound **2**.

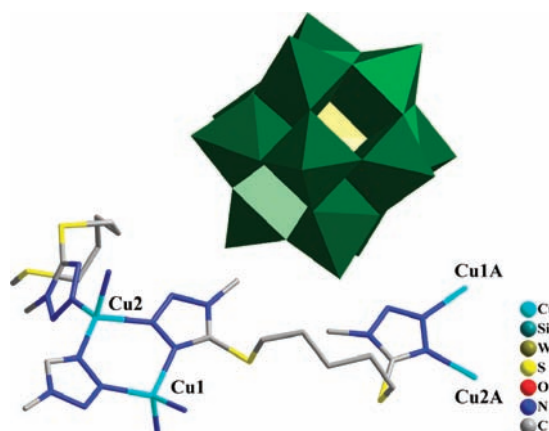


Figure 7. Stick/polyhedral view of the asymmetric unit of compound **3**. H atoms are omitted for clarity.

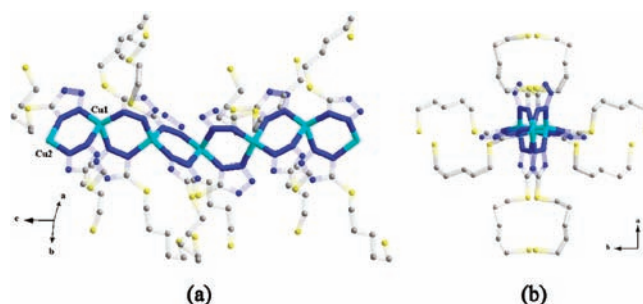


Figure 8. Fragment of the cationic chain in the structure of **3** (a), showing the inversion center of the Cu axis (b).

bridging μ_4 -bmtp ligands and the Cu2 atoms, as shown in Figure 9 (right).

Influence of the Flexible Tetrazole-Based Thioethers on the Metal–Organic Networks. In this work, we selected three kinds of flexible S-containing bis(tetrazole) ligands (bmtm, bmte, and bmtp), intending to observe their effect on the assembly of the POM-based hybrids. Compared with commonly used flexible organic ligands, dramatic changes of these organic ligands are as follows: (i) the introduction of a soft S atom; (ii) utilization of the tetrazole ring with more potential coordination sites; (iii) alteration of the spacer length and steric hindrance.

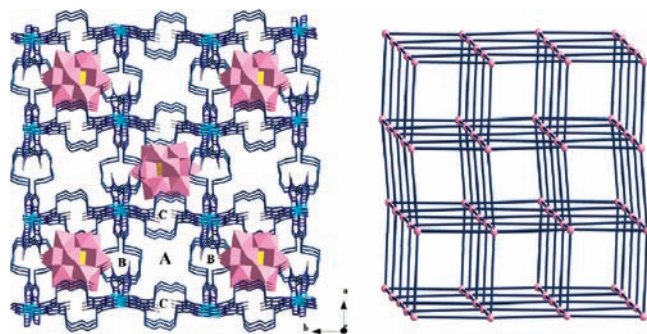


Figure 9. Left: POM-templated 3D host framework with a large cavity (A-type) and two types of small windows (B and C types). For clarity, some A-type voids are pictured as empty and the H atoms have been omitted. Right: Schematic view of a six-connected host framework with a primitive (α -Po) net in compound **3**.

First, the introduction of a soft S atom brings the ligands more flexibility and conformational freedom. In compound **1**, the $-\text{S}(\text{CH}_2)\text{S}-$ backbone makes it easier for the bmtm molecule to chelate a Cu^{I} ion, forming a stable eight-membered chelating cycle. Remarkably, no bmtm molecule in compound **1** prefers to act as the bridging linker. The main reason should be attributed to the flexible nature of the bmtm ligand. In compound **2**, the bmtm ligand has a longer $-\text{S}(\text{CH}_2)_2\text{S}-$ backbone. The distance of the two apical coordinated N atoms from bmtm¹ is beyond 9.4 Å (Figure S5a in the Supporting Information). However, half of the bmtm ligands (bmtm³ and bmtm⁴) twist their backbones deeply to chelate Cu^{I} ions, forming stable nine-membered chelating rings. The terminal N atoms span a short distance of ~ 3.6 – 3.7 Å (Figure S5b in the Supporting Information). Examples of flexible ligands with a $-(\text{CH}_2)_4-$ backbone acting as chelators have not been observed in previous studies.^{7b,c,8a,17}

In compound **3**, the bmtm molecule has the longest $-\text{S}(\text{CH}_2)_5\text{S}-$ backbone. Such flexible linkers span the binuclear units within the network at distances of ~ 12.9 – 13.4 Å (Figure S6 in the Supporting Information). Obviously, from a structural point of view, it is unlikely for such a long ligand to act as a chelator, and all of the bmtm ligands in **3** do exist as bridging linkages. Notably, owing to different soft degrees of the S and C atoms, the rotation angles around the S atoms are obviously smaller than those of the C atoms. The average deviation is up to 13.9° . A similar phenomenon has also been observed in **1** and **2** with average deviations of 15.3° and 10.6° , respectively (Table S2 in the Supporting Information).

Second, utilization of the tetrazole ring provides more potential coordination sites. A consequence of this feature is that the coordination capacity of organic ligands is strongly enhanced. The diverse coordination modes and conformations created under the self-assembly process support this conclusion. In compound **1**, two types of bmtm molecules with different conformations are observed, which utilizes half of its available N donors to coordinate to Cu^{I} ions in a uniform $\mu_2(\eta^1, \eta^2)$ fashion. It is worth mentioning here a S atom from bmtm¹, which acts as an important S bridge, leading to a special $\mu_3(\eta^1, \eta^2, \eta^1_s)$ fashion. In compound **2**, four types of coordination modes of the bmtm ligand are observed, namely, $\mu_2(\eta^1, \eta^1)$, $\mu_3(\eta^1, \eta^2)$, $\mu_3(\eta^1, \eta^3)$, and

$\mu_3(\eta^2, \eta^2)$ fashions. Such an unusual phenomenon coexisting in one structure should be assigned to the powerful coordination capacity of the organic ligands. In compound **3**, there are also two types of bmtm molecules with different conformations and distinct $\mu_4(\eta^2, \eta^2)$ coordination fashions. In summary, eight coordination modes of flexible bis(tetrazole) ligands within three compounds further enrich the coordination chemistry and sufficiently prove our rational synthetic strategy.

Third, alteration of the spacer length has a great influence on the frameworks of the title compounds. First, the molar ratio of chelating-to-bridging ligands decreases as the spacer length is increased. The molar ratio is 4:0 in **1**, 2:2 in **2**, and 0:4 in **3**, which can be best illustrated by the structure stability. Second, the role of POM clusters changes from inorganic building block to noncoordinating template. In compound **1**, the SiW_{12} clusters act as tetradentate inorganic ligands to connect four Cu^{I} ions. In **2**, bidentate and tetradentate linkages of SiW_{12} clusters coexist. However, in **3**, the SiW_{12} clusters act as noncoordinating templates rather than covalent linkers. A tendency is that the longer the $-\text{S}(\text{CH}_2)_n\text{S}-$ spacer, the bigger the steric hindrance of organic ligands and the weaker the coordination capacity of POM.^{7c}

Multimetalloccyclic Units. In coordination chemistry, long and flexible ligands have the potential for the assembly of novel entangled structures with interpenetrating character;^{9e,f,18} such a phenomenon could be recognized as self-complementary of the structure stability. In this work, flexible bis(tetrazole) ligands induce metal ions, forming uncommon multimetalloccyclic units, which play a key role in enhancing the stability of the whole network. In compound **1**, the bimetalloccyclic unit is observed (Figure S7a in the Supporting Information), which is constructed by two types of metalloccyclic (MC) rings. The first one is a six-membered dinuclear ring (MC-2); without a doubt, the hexagon is one of the most stable configurations. The second one is an eight-membered chelating ring (MC-3). In **2**, three types of MCs formed a tetrametalloccyclic unit (Figure S7b in the Supporting Information), composed of one five-membered dinuclear ring (MC-1), two MC-2, and two nine-membered chelating rings (MC-4). In **3**, three kinds of octametalloccyclic units are observed (Figure S7c,d in the Supporting Information), which could be considered the basic building blocks of the 3D framework. Besides stable hexagon rings within these octametalloccyclic units, three macrocycles coexist, namely, a 30-membered macrocycle (MC-6), a 33-membered macrocycle (MC-7), and a 34-membered macrocycle (MC-5). Thus, such multimetalloccyclic units within compounds **1**–**3** play a key role in stabilizing the whole structure.

TGA. The thermal behavior of compounds **1**–**3** was studied by TGA. The experiments were performed under a N_2 atmosphere with a heating rate of $10^\circ\text{C}/\text{min}$ in the temperature range of 30 – 800°C for compounds **1**–**3**, as shown in Figure S9 in the Supporting Information. For compound **1**, the water molecules were eliminated from the

(17) (a) Zhang, W. L.; Liu, Y. Y.; Ma, J. F.; Jiang, H.; Yang, J.; Ping, G. J. *Cryst. Growth Des.* **2008**, *8*, 1250. (b) Liu, X. G.; Wang, L. Y.; Zhu, X.; Li, B. L.; Zhang, Y. *Cryst. Growth Des.* **2009**, *9*, 3997.

(18) (a) Batten, S. R. *CrystEngComm* **2001**, *18*, 1. (b) Gu, Z. G.; Xu, Y. F.; Zhou, X. H.; Zuo, J. L.; You, X. Z. *Cryst. Growth Des.* **2008**, *8*, 1306. (c) Adarsh, N. N.; Dastidar, P. *Cryst. Growth Des.* **2010**, *10*, 483. (d) Li, Q. W.; Zhang, W. Y.; Miljanić, O. S.; Knobler, C. B.; Stoddart, J. F.; Yaghi, O. M. *Chem. Commun.* **2010**, *46*, 380.

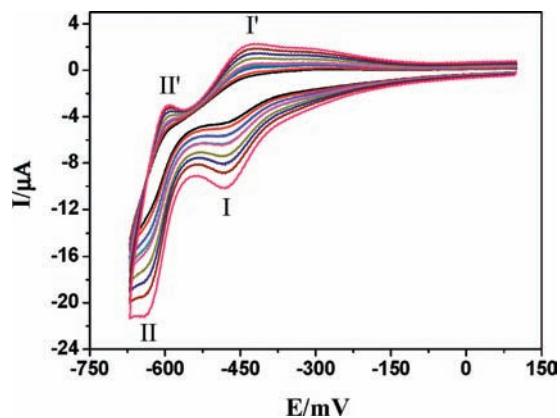


Figure 10. Cyclic voltammograms of **2**-CPE in a 1 M H₂SO₄ solution at different scan rates (from inner to outer: 100, 120, 140, 160, 180, 200, 250, 300, and 350 mV/s).

network (calcd 0.87%; found 1.10%) when the temperature was increased to about 200 °C, after which removal of the organic components (~280 °C) and collapse of the Keggin-type SiW₁₂ clusters (~530 °C) occurred. The complete decomposition was finished up to 800 °C (calcd 23.57%; found 23.65%). For compounds **2** and **3**, the removal of organic components occurred at 300 and 275 °C, respectively. Collapse of the SiW₁₂ clusters occurred at about 570 °C for **2** and 600 °C for **3**, and the complete decomposition of the SiW₁₂ clusters was finished up to ~650 °C for **2** and 700 °C for **3**, respectively. The total weight loss was consistent with the calculated values (calcd 22.39%, found 22.08% for **2**; calcd 27.71%, found 27.05% for **3**).

Electrochemical Properties. The electrochemical properties of compounds **1–3** were studied in a 1 M H₂SO₄ aqueous solution. The results exhibited almost no structural effect on the redox property, except for some slight potential shifts of the redox peaks (Figure S10 in the Supporting Information). Therefore, only cyclic voltammograms for **2**-CPE at different scan rates are described here as an example.

The cyclic voltammograms for **2**-CPE in a 1 M H₂SO₄ aqueous solution at different scan rates are presented in Figure 10. In the potential range of -700 to +100 mV, there are two pairs of reversible redox peaks, I–I' and II–II', with the mean peak potentials $E_{1/2} = (E_{pc} + E_{pa})/2$ at -456 and -617 mV (scan rate: 120 mV/s), respectively, which should be ascribed to redox of the SiW₁₂ anion.^{6b,19} With the scan rates increasing, the peak potentials changed gradually: the cathodic peak potentials shifted to the negative direction and the corresponding anodic peak potentials toward the positive direction. The peak-to-peak separation between the corresponding cathodic and anodic peaks increases, but the mean peak potential does not change on the whole. The peak currents are proportional to the scan rates up to 400 mV/s, suggesting that the redox process is surface-controlled (Figure S11 in the Supporting Information).

As is well-known, the electroreduction of nitrite requires a large overpotential;²⁰ therefore, no obvious

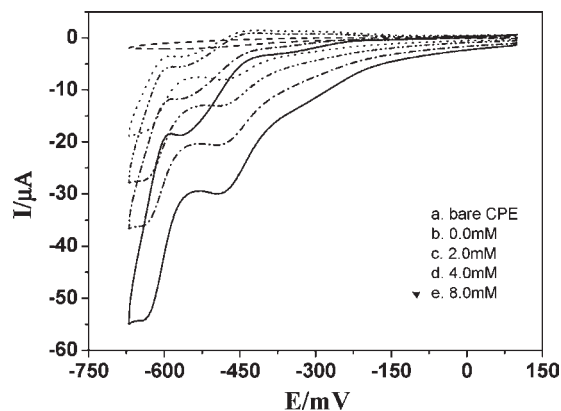


Figure 11. Cyclic voltammograms of **2**-CPE in a 1 M H₂SO₄ solution containing 0.0–8.0 mM KNO₂ and a bare CPE in a 6 mM KNO₂ + 1 M H₂SO₄ solution. Potentials vs SCE. Scan rate: 120 mV/s.

response is observed at the presence of nitrite in the potential range of -700 to +100 mV at a bare CPE. However, at **2**-CPE, with the addition of nitrite, all of the reduction peak currents increase gradually while the corresponding oxidation peak currents decrease, which indicates that the reduction of nitrite is mediated by the reduced species of SiW₁₂ anions and **2**-CPE displays good electrocatalytic activity toward the reduction of nitrite (Figure 11).

Conclusion

In summary, three POM hybrids based on copper(I) bis-(tetrazole) metal–organic units and SiW₁₂ clusters have been synthesized under hydrothermal conditions. Compound **1** exhibits unusual Cu–S bonds, which are scarce in POM chemistry. Compound **2** possesses the highest connection number and the unique connection fashion of saturated Keggin-type POMs. Compound **3** represents a POM-templated 3D framework with two types of small windows radially arranged within the whole 3D structure. It is found that the nature of the bis(tetrazole) ligand plays a crucial role in the assembly of title compounds, which is reflected in three aspects: (i) the introduction of soft S atoms intensifies the flexibility greatly; (ii) utilization of tetrazole rings endows the ligand with strong coordination ability; (iii) alteration of the flexible -S(CH₂)_nS- backbones makes ligands with different spacer lengths and steric hindrance. This work, to some extent, provides a good example of reasonable design and controllable assembly of POM-based metal–organic networks. Besides enriching the POM family, with hindsight, our work will open opportunities for investigating novel POM-based hybrid materials within such a system in the long term. These efforts are currently ongoing.

Acknowledgment. Financial support of this research by Grant NCET-09-0853, the National Natural Science Foundation of China (Grant 20871022), and the Foundation of Liaoning Province (Grant 2009R03) is greatly acknowledged.

Supporting Information Available: X-ray crystallographic information files (CIF), tables of selected bond lengths and angles, and structural figures of compounds **1–3**, together with IR, XPS, TGA, and cyclic voltammetry data. This material is available free of charge via the Internet at <http://pubs.acs.org>.

(19) (a) Sha, J. Q.; Peng, J.; Tian, A. X.; Liu, H. S.; Chen, J.; Zhang, P. P.; Su, Z. M. *Cryst. Growth Des.* **2007**, *7*, 2535. (b) Sadakane, M.; Steckhan, E. *Chem. Rev.* **1998**, *98*, 219.

(20) Keita, B.; Nadjo, L. J. *Electroanal. Chem.* **1987**, *227*, 77.